CRYSTAL GROWTH & DESIGN

ARTICLE

pubs.acs.org/crystal

Multinuclear Solid-State Magnetic Resonance and X-ray Diffraction Study of Some Thiocyanate and Selenocyanate Complexes Exhibiting Halogen Bonding

Published as part of the Crystal Growth & Design virtual special issue on Halogen Bonding in Crystal Engineering: Fundamentals and Applications

Jasmine Viger-Gravel, Ilia Korobkov, and David L. Bryce*

University of Ottawa, 10 Marie Curie Private, Ottawa, Ontario, Canada K1N 6N5

Supporting Information

ABSTRACT: We report on the preparation and study of a series of thiocyanate and selenocyanate compounds exhibiting halogen bonding between iodine and nitrogen, sulfur, or selenium. The novel compounds $(Me_4NSeCN)(p\text{-}C_6F_4I_2)_2$ (**1**), $(Me_4NSeCN)(o\text{-}C_6F_4I_2)_2$ (**2**), and $(Me_4NSCN)(p\text{-}C_6F_4I_2)_2$ (**4**) were synthesized. Their crystal structures and local halogen bonding interactions, along with those of related additional thiocyanate and selenocyanate compounds (e.g., KSCN, Me_4NSCN, Me_4NSeCN, etc.) were investigated by single-crystal X-ray diffraction and multinuclear ($^{13}C/^{15}N/^{77}Se$) solid-state magnetic resonance spectroscopy. Compounds **1** and **2** exhibit trifurcated I···$SeCN^-$ close contacts with characteristic bonding angles near 90°. X-ray and $^{13}C/^{15}N$ solid-state NMR evidence indicates that the thiocyanate moieties in **4** exhibit 2-fold disorder. The utility of $^{13}C/^{14}N$ dipolar coupling and residual dipolar coupling data is discussed. ^{14}N solid-state NMR spectroscopy is found to be impractical in the compounds of interest due to fast T_2 relaxation. ^{13}C chemical shifts of the thiocyanates are observed to increase slightly in complexes exhibiting halogen bonding relative to reference compounds with only simple counterions, while ^{15}N chemical shifts decrease slightly under the same conditions. The opposite trends are noted for the selenocyanates. More substantial changes are observed in both the ^{77}Se isotropic chemical shift and in the pseudounique principal component of the ^{77}Se chemical shift tensor when comparing simple selenocyanates with those where the ^{77}Se is engaged in halogen bonding interactions with iodine. These results are interpreted in the context of Ramsey's theory to show that the iodine—selenium interactions are reflected in the ^{77}Se solid-state NMR parameters, thereby providing an example of the utility of NMR methods in characterizing halogen bonding interactions in the solid state.

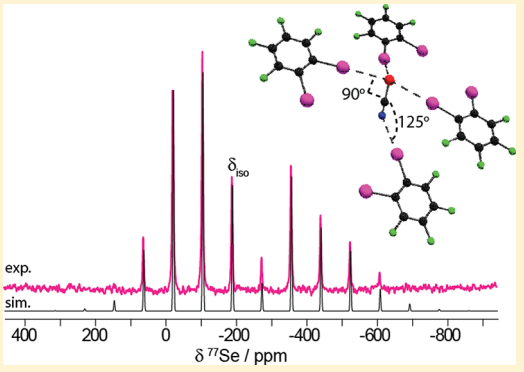

INTRODUCTION

A classic example of the concept of halogen bonding is found in the donor—acceptor complex of I_2 and benzene,[1,2] where in the 1950s the interaction was described as weak charge-transfer bonding. Until the 1990s, the halogen bonding mechanism in molecular self-assembly and recognition was still not completely understood.[3] In the past decade, many studies have been conducted on halogen bonding in crystal engineering for supramolecular chemistry.[4] Halogen bonding has proven to be a moderately strong (10 to 200 kJ mol^{-1}),[5] specific, and highly directional interaction.[6] This interaction has a direct impact on research fields where molecular recognition and self-assembly processes are important. Halogen bonding,[6] RX···B, is the result of a noncovalent interaction between a halogen, X, and an electron-rich site, B (e.g., Lewis base or π electrons). The halogen is part of an RX molecule where R can be another halogen, an organic or an inorganic electron-donating group.[6,7,9] These interactions are considered as significant since the X···B distance is shorter than the sum of the van der Waals radii of the two atoms involved (1.75, 1.85, 1.98 Å for Cl, Br, and I, respectively, and 1.70, 1.74, 2.00 Å for N, S, and Se, respectively).[8] It has been observed that a nucleophile will typically align with RX in an almost linear fashion (160−180°), whereas an electrophile will align at an angle varying between 90 and 120°.[6,7,9] The molecular orbitals centered on a halogen are qualitatively viewed as being negative in character (negative electrostatic potential), in the context of an RX−B compound. However, extensive studies of the electrostatic potential surface demonstrate a positive region at the outermost part of the R−X bond surrounded by negative electrostatic potential. This positive region is known as the σ-hole, and its magnitude depends on the nature of the halogen nucleus and the electron-withdrawing power of R.[7] The potency of the halogen bonding interaction increases in the order Cl < Br < I. Fluorine is typically less active since it lacks a prominent

Received: July 13, 2011
Revised: September 7, 2011
Published: September 12, 2011

σ-hole due to its high electronegativity and high sp hybridization.[7] The interaction has been observed in cases of molecular folding[10] and recognition,[11,12] ligand binding,[13] and in the assembly of host−guest solids.[14] These examples demonstrate that halogen bonding can play a key role in the design of new drugs and inhibitors.[15−17] Halogen bonding is also being exploited in materials chemistry.[18−20] The interaction can induce cocrystallization with specific spatial orientations of the components.[6,21]

Recently, Cauliez et al. published a report on the thiocyanate anion as a polydentate halogen bond acceptor.[22] The compounds they studied had the form $(R_4NSCN)_x$ (*ortho* or *para* − $C_6F_4I_2)_y$ and $(R_4NSCN)_x$(*sym* − $C_6F_3I_3)_y$. They determined that both the sulfur and nitrogen atoms of the thiocyanate moiety engage in halogen bonding interactions as previously described by Bock and Holl for tetraiodoethylene, tetraiodothiophene, and *N*-methyltetraiodopyrrole.[23] However, Cauliez et al. observed C−S···I bond angles of about 90° as well as multiple iodines interacting with sulfur and strong deviations from linearity in the C≡N···I interactions (145−170°).[22] These interesting results prompted us to initiate an investigation of similar compounds, $(R_4NSCN)_x(p\text{-}C_6F_4I_2)_y$ and $(R_4NSeCN)_x$(*o*- or *p*-$C_6F_4I_2)_y$, with a focus on the potential information which may be available through solid-state nuclear magnetic resonance (SSNMR) spectroscopy and on the interaction motifs of the selenocyanate ion versus the thiocyanate ion. Selenium has been observed to participate in halogen bonding in a mutant form of T4 lysozyme, selenoethers, and selenoamides.[6,12,24] SSNMR powder lineshapes provide a wealth of structural information and insight into the interactions which are characteristic of a particular nuclear environment, such as dipolar coupling (D) and chemical shift anisotropies (CSA).[25] With four readily observable NMR-active nuclei (^{13}C, $^{14/15}$N, and ^{77}Se) involved directly and indirectly in this noncovalent interaction in our compounds of interest, a good deal of information may potentially be gained from their chemical shift (CS) tensors. Furthermore, acquisition of natural-abundance SSNMR spectra of ^{13}C, ^{15}N, and ^{77}Se is straightforward due to the use of cross-polarization[26] (CP) from ^{1}H. We note in passing that while there have been recent advances in ^{127}I SSNMR,[27] observing NMR spectra for covalently bound iodine remains impractical.[27,28]

In the current work, we investigate the effects of halogen bonding on the compounds mentioned above using X-ray crystallography, multinuclear solid-state magnetic resonance, and quantum chemistry. We describe possible correlations between halogen bonding and the NMR parameters. Results are compared with those for simple thiocyanate and selenocyanate salts.

EXPERIMENTAL SECTION

1. Synthesis. *n*-Bu_4NSCN was purchased from Aldrich whereas ^{13}C isotopically enriched KSCN (99.99%) and ^{15}N isotopically enriched KSCN (>98%) were purchased from ISOTEC, and all compounds were used without further purification. Me_4NSCN, $Me_4NS^{13}CN$, $Me_4NSC^{15}N$, and Me_4NSeCN were synthesized according to published procedures.[29] Melting points were measured and found to be consistent with those previously reported,[30] and crystal structures were also solved using single-crystal X-ray diffraction. (*n*-$Bu_4NSCN)(p\text{-}C_6F_4I_2)$ (**3**) was synthesized as described by Cauliez et al.[22] The halogenated compounds $(Me_4NSCN)(p\text{-}C_6F_4I_2)_2$ (**4**), $(Me_4NSeCN)(p\text{-}C_6F_4I_2)_2$ (**1**), and $(Me_4NSeCN)(o\text{-}C_6F_4I_2)_2$ (**2**) were synthesized by dissolving the relevant compounds in a minimum amount of warm EtOH (95%), using a warm water bath (50 °C). For each synthesis, 2 equiv of *p*-diiodotetrafluorobenzene or *o*-diiodotetrafluorobenzene was mixed with 1 equiv of $Me_4NS^{13}CN$, $Me_4NSC^{15}N$, or Me_4NSeCN, respectively. See the Supporting Information for further details.

2. X-ray Crystallography. Crystal structures were collected at the University of Ottawa in the X-ray diffraction Laboratory. Data collection results for compounds **1**, **2**, and **4** represent the best data sets obtained in several trials for each sample. The crystals were mounted on thin glass fibers using paraffin oil. Data for **4** were collected at 296.15 K. Crystals of the other two compounds were cooled to 200.15 K prior to data collection. Data were collected on a Bruker AXS SMART single crystal diffractometer equipped with a sealed Mo tube source (wavelength 0.71073 Å) APEX II CCD detector. Raw data collection and processing were performed with the APEX II software package from Bruker AXS.[31] Diffraction data for **1** and **4** were collected with a sequence of 0.5° ω scans at 0, 120, and 240° in φ. Diffraction data for **2** were collected with a sequence of 0.5° ω scans at 0, 90, 180, and 270° in φ due to the lower symmetry of the crystal unit cell to provide adequate data coverage. Initial unit cell parameters were determined from 60 data frames collected for different sections of the Ewald sphere. Semiempirical absorption corrections based on equivalent reflections were applied.[32] Systematic absences in the diffraction data set and unit cell parameters were consistent with monoclinic $C2/c$ (No. 15) for compound **4**, monoclinic $P2_1/n$ (No. 14) for compound **1**, and triclinic $P\bar{1}$ (No. 2) for compound **2**. Solutions in the centrosymmetric space groups for all compounds yielded chemically reasonable and computationally stable refinement results. All hydrogen atoms were treated as idealized contributions. All scattering factors are contained in several versions of the SHELXTL program library, with the latest version used being v.6.12.[33] Crystallographic data and selected data collection parameters are reported in Table 1.

3. Solid-State NMR Spectroscopy. Static, magic-angle spinning (MAS), CP, and Hahn-echo SSNMR experiments were used for the characterization of the halogenated compounds of the form $(R_4NSeCN)_x$(*o*- or *p*-$C_6F_4I_2)_y$ and $(R_4NSCN)_x(p\text{-}C_6F_4I_2)_y$ and the ammonium thiocyanate or selenocyanate salts of the form R_4NSCN or R_4NSeCN. Samples were powdered and packed in 7 and 4 mm o.d. zirconium oxide rotors.

4.7 T Data. The majority of the SSNMR experiments for ^{13}C (ν_L = 50.307 MHz) were conducted on a Bruker Avance III 200 MHz wide bore spectrometer (4.7 T) equipped with a 7 mm triple resonance HXY MAS probe or wide-line probe. Experimental setup and pulse calibrations were performed using glycine, the secondary standard for ^{13}C. The carbon chemical shifts were referenced to TMS by setting the chemical shift of the carbonyl peak of solid glycine to 176.4 ppm.[34]

A Hahn-echo (i.e., $\pi/2$-τ_1-π-τ_2-acq)[26] pulse sequence was used for the acquisition of a ^{13}C NMR spectrum of 99.9% ^{13}C-enriched powdered KSCN under stationary conditions. Parameters used were 4 μs 90° pulse length, 120 s recycle delay, and 1329 scans were collected for a total of 44 h of experimental time.

For CP experiments, the recycle delay used was 2 s for R_4NSCN and R_4NSeCN, and 14 s for the halogenated compounds. A contact time of 12 ms was optimized on Me_4NSCN. The proton 90° pulse lengths used were all ~3.5 μs. MAS spinning frequencies were 5 kHz. Total experimental time ranged from 1 to 3 h for MAS experiments and 21 to 44 h for static experiments. Proton decoupling using the SPINAL-64[35] method was applied during acquisition of the spectra of all samples.

9.4 T Data. ^{13}C (ν_L = 100.613 MHz), ^{77}Se (ν_L = 76.311 MHz), and ^{15}N (ν_L = 40.56 MHz) SSNMR experiments were carried out on a 400 MHz (B_0 = 9.4 T) Bruker Avance III wide-bore spectrometer equipped with a triple resonance 4 mm HXY MAS probe. Experimental setup and pulse calibration were performed using the recommended IUPAC standards for ^{13}C, ^{15}N, and ^{77}Se.[36,37] Nitrogen chemical shifts were referenced to NH_3 (*l*, 293 K) by setting the chemical shift of the ammonium peak in solid ammonium nitrate, $^{15}NH_4NO_3$, to 23.8 ppm.[36]

dx.doi.org/10.1021/cg200889y |*Cryst. Growth Des.* 2011, 11, 4984–4995

Table 1. Crystallographic Data and Selected Data Collection Parameters

compound	1	2	4
empirical formula	$C_{17}H_{12}F_8I_4N_2Se$	$C_{17}H_{12}F_8I_4N_2Se$	$C_{17}H_{12}F_8I_4N_2S$
formula weight	982.85	982.85	935.95
crystal size, mm	0.20 × 0.17 × 0.17	0.27 × 0.17 × 0.17	0.24 × 0.17 × 0.13
crystal system	monoclinic	triclinic	monoclinic
space group	$P2_1/n$ (No. 14)	$P\bar{1}$ (No. 2)	$C2/c$ (No. 15)
Z	4	2	4
a, Å	9.4954(3)	8.7214(7)	12.2784(3)
b, Å	24.6517(8)	11.0795(9)	9.0581(3)
c, Å	11.4085(4)	13.4793(11)	23.5345(6)
α, °	90	93.753(4)	90
β, °	103.240(1)	90.429(4)	94.268(2)
γ, °	90	97.315(4)	90
volume, Å^3	2599.49(15)	1288.95(18)	2610.22(13)
calculated density, Mg/m^3	2.511	2.532	2.382
absorption coefficient, mm^{-1}	6.260	6.313	4.920
F(000)	1784	892	1712
Θ range for data collection, °	2.01−28.30	2.32−28.35	2.80−26.47
limiting indices	$h = \pm 10$, $k = \pm 21$, $l = \pm 15$	$h = \pm 11$, $k = \pm 14$, $l = \pm 17$	$h = \pm 15$, $k = \pm 11$, $l = \pm 29$
reflections collected/unique	16148/6393	26961/6346	15607/2681
R(int)	0.0183	0.0262	0.0273
completeness to Θ = 28.32, %	98.9	98.4	98.8
max and min transmission	0.4158 and 0.3674	0.4941 and 0.2906	0.5672 and 0.3847
data/restraints/parameters	6393/0/289	6346/0/289	2681/0/159
goodness-of-fit on F^2	1.018	1.073	1.022
final R indices [$I > 2\sigma(I)$]	$R_1 = 0.0276$, $wR_2 = 0.0621$	$R_1 = 0.0228$, $wR_2 = 0.0573$	$R_1 = 0.0289$, $wR_2 = 0.0760$
R indices (all data)	$R_1 = 0.0379$, $wR_2 = 0.0656$	$R_1 = 0.0255$, $wR_2 = 0.0588$	$R_1 = 0.0394$, $wR_2 = 0.0826$
largest diff peak/hole, e·Å^{-3}	0.477/−0.946	0.907/−1.382	0.555/−0.646

Solid diammonium selenate, $(NH_4)_2SeO_4$, (δ_{iso} = 1040.2 ppm), was used to reference the chemical shift of selenium with respect to $Se(CH_3)_2$ (l).[37] The contact times used for ^{13}C and ^{15}N CP experiments were optimized on labeled ^{13}C and ^{15}N Me_4NSCN and found to be 13 and 18 ms, respectively. For ^{77}Se NMR experiments, the recycle delay and contact time used were 5 s and 30 ms, respectively. The ^1H 90° pulse lengths used for the CP experiments were ∼3 to 4 μs in all cases. Proton decoupling using the CW,[38] SPINAL-64,[35] or TPPM[39] methods was applied during acquisition of the spectra of all samples. In the case of ^{15}N, low decoupling powers were needed to observe the ammonium peak of the R_4NSCN (R = Me, *n*-Bu) and Me_4NSeCN salts; this is consistent with motion of the R_4N^+ groups.[40] For CPMAS experiments on ^{13}C and ^{15}N, the MAS frequencies ranged between 2 and 8 kHz. For ^{77}Se, MAS frequencies ranged from 6 to 10 kHz. Total experimental time for ^{13}C CPMAS experiments varied between 15 min and 3 h, and static experiments lasted 20 h. Natural abundance ^{15}N experiments necessitated 12 to 44 h for signal averaging, whereas ∼50% isotopically enriched samples needed 1 h for Me_4NSCN to 40 h for compound **4**. Experiment times for the ^{77}Se SSNMR experiments ranged from 5 min (Me_4NSeCN) to 1 day (**1** and **2**). Complementary data collected at 11.75 T may be found in the Supporting Information.

21.1 T Data. ^{14}N SSMNR experiments were performed using the 900 MHz (B_0 = 21.14 T) Bruker Avance II spectrometer at the National Ultrahigh-Field NMR Facility for Solids in Ottawa ($\nu_L(^{14}N)$ = 65.046 MHz) using a Bruker Avance II console and a 7.0 mm HX static probe built in-house. The WURST-QCPMG pulse sequence,[41] which combines the broadband excitation and refocusing capabilities[42] of frequency swept wideband, uniform rate, smooth truncation (WURST) pulses[43] with the signal enhancement of the quadrupolar Carr-Purcell-Meiboom-Gill (QCPMG) protocol, was used.[44] For KSCN, the variable offset method was used with 100 kHz intervals and 10 pieces acquired, giving half of the spectrum. Each piece was collected with a spectral window of 2 MHz, 256 scans, and 64 echoes per scan. The parameters used were 10 s recycle delay, 50 μs WURST pulse, and 5 kHz spikelet separation.

Spectral Processing and Simulation. NMR spectra were processed using the Bruker TopSpin 3.0 program. For variable offset spectra, the different pieces were coadded to produce the whole spectrum. Spectral simulations were performed using WSOLIDS1,[45] which incorporates the space-tiling algorithm of Alderman et al.[46] The spinning sidebands observed in the CPMAS NMR spectra were analyzed to obtain the CSA using the procedure of Herzfeld and Berger[47] with the program HBA.[48] The fit was then verified and refined using WSOLIDS1. Stack plots were produced using DMFit2010.[49]

4. Computational Details. A model was generated from the X-ray crystal structure atomic coordinates for each halogenated compound using one SCN^- or $SeCN^-$ anion and the nearest interacting (*p* or *o*)-diiodotetrafluorobenzene moieties, where the X-ray structure demonstrates characteristic halogen bonding distances and angles. ^{77}Se magnetic shielding tensors were calculated for those models with the Gaussian 09 program.[50] The hybrid DFT functional, B3LYP,[51] was used for all calculations. A study of different basis sets was conducted and 6-311++G** was found to provide the most reliable results. A smaller basis set was used for iodine (6-311G**).

The shielding tensors contained in the Gaussian 09 output files were analyzed using a modified version of the EFGShield program (version 1.1).[52] The absolute shielding scale for ^{77}Se was used to convert shielding constants to chemical shifts.[53]

RESULTS AND DISCUSSION

1. X-ray Crystal Structures. The X-ray crystal structures of the halogen compounds **1**, **2**, **3**, and **4** were collected. The crystallographic data for the new compounds may be found in Table 1. Halogen bonding interactions are inferred from the observed short interatomic distances when compared with the sum of the van der Waals radii (I···N: 3.68 Å, I···S: 3.72 Å, and I···Se: 3.98 Å) or with the sum of the nonisotropic radii of Nyburg and Faerman[54] (I···N: 3.36 Å, I···S: 3.79 Å, and I···Se: 3.91 Å) (see also the Supporting Information). As mentioned, halogen bonding is a highly directional interaction; the thiocyanate anion demonstrates bidentate character with ∼90° bond angles for I···S−C and angles of 145 to 170° for I···N−C.[23,22] For selenocyanate, one may anticipate observing I···Se−C angles varying between 90° and 120° in halogen bonding interactions, as selenium is analogous to sulfur. Interatomic N···I, S···I, and Se···I distances as well as I···N−C, I···S−C, and I···Se−C angles are presented in Table 2 for each compound. A description of the solid state structural motifs and correlations to halogen bonding interactions follows.

Table 2. Selected Intermolecular Contact Distances (Å) and Angles (°)

compound	$d_{I\cdots N}$	$\theta_{I\cdots NC}$	$d_{I\cdots Se}$	$\theta_{I\cdots SeC}$
1	3.034	125.76	3.393	111.72
			3.421	83.91
			3.405	86.98
2	3.035	124.13	3.404	80.95
			3.552	89.95
			3.401	94.01
compound	$d_{I\cdots N}$	$\theta_{I\cdots NC}$	$d_{I\cdots S}$	$\theta_{I\cdots SC}$
3	2.911	169.19	3.249	87.51
4	3.275	114.11	3.277	104.23
	3.107	104.67	3.313	94.59

As mentioned, compound **3** ((*n*-Bu_4NSCN)(*p*-$C_6F_4I_2$)) has previously been characterized by Cauliez et al.;[22] the complex synthesized in our laboratory presents the same unit cell parameters. The halogen bonding occurring in this compound is consistent with that previously reported: the thiocyanate anion acts as a bidentate ligand forming long chains separated by the bulky tetrabutylammonium cation. The motif can be seen in Figure 1a. The related compound **4** crystallizes in a monoclinic system with the *C*2/*c* space group. Disorder is present in the crystal structure, as the SCN^- anion may be aligned in two different directions. Figure 1b shows the two possible orientations that thiocyanate can take in the unit cell. In one unit cell, the SCN^- ion is oriented in a unique direction, and it is clear that either way the linear anion is placed, the I···N and I···S short contacts remain the same due to symmetry. It is the random position of SCN^- in the adjacent unit cell which could affect the NMR interaction tensors of the first SCN^- moiety; a broadened resonance could be observed in the ^{13}C and ^{15}N SSNMR spectra of **4** (vide infra). The *p*-$C_6F_4I_2$ molecules form unaligned columns along the *b* axis, and the cations (Me_4N^+) are located between those columns and alternate with the SCN^- anion (Figures S2 and S3, see Supporting Information). Nitrogen and

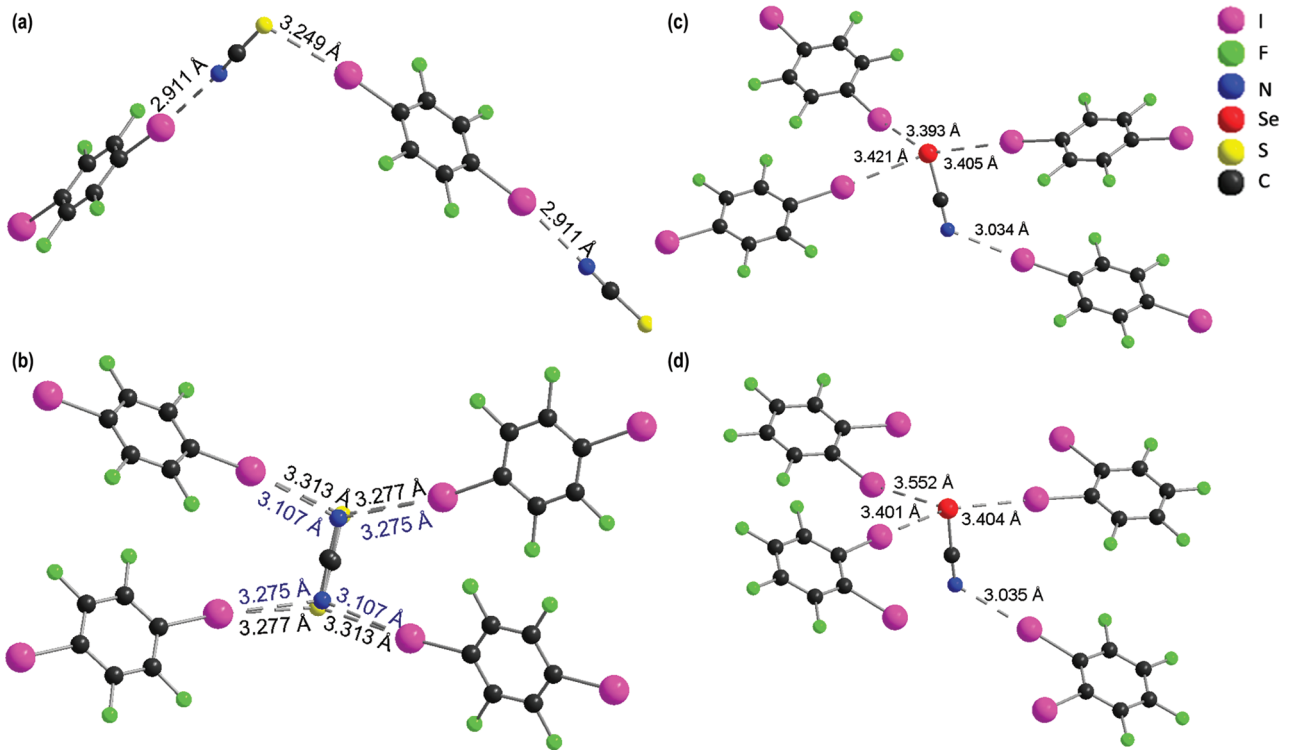

Figure 1. Halogen bonding environments around the thiocyanate and selenocyanate anions in compounds **1**−**4**. (a) A view of a chain formed by the bidentate SCN^- anion in compound **3**, (*n*-Bu_4NSCN)(*p*-$C_6F_4I_2$), along the *b* axis.[22] (b) Projection view along the *b* axis of the disordered compound **4**, (Me_4NSCN)(*p*-$C_6F_4I_2$)$_2$ (short contact distance in blue text corresponds to I···N and black corresponds to I···S) and (c) of one layer of **1**, (Me_4NSeCN)(*p*-$C_6F_4I_2$)$_2$ and (d) **2**, (Me_4NSCN)(*o*-$C_6F_4I_2$)$_2$ showing the halogen bonds with SCN^-. The R_4N^+ cations have been omitted for clarity.

dx.doi.org/10.1021/cg200889y |*Cryst. Growth Des.* 2011, 11, 4984–4995

sulfur both interact with two iodines, as shown in Figure 1b. In this compound, **4**, it is not clear if nitrogen is part of a halogen bond according to the definition, since the I···N−C angles are far from linear (114.1° and 104.7°). However, the interactions between iodine and nitrogen are not negligible (as inferred from the internuclear distances of 3.275 Å and 3.107 Å). In the case of sulfur, the interatomic distances ($d_{I\cdots S}$: 3.313 Å and 3.277 Å) and angles ($\theta_{I\cdots S-C}$: 104.2° and 94.6°) are both typical of halogen bonding. The overall crystal packing motif for **4** is shown in the Supporting Information. Briefly, the packing consists of alternating layers of *p*-diiodotetrafluorobenzene and charged moieties. The layers consisting of the charged species alternate between cation (Me_4N^+) and anion (SCN^-). In addition, the aromatic molecules are oriented in two different directions, which is concomitant with the halogen bonding interactions between the iodine and thiocyanate.

Conversely, no orientational disorder of the selenocyanate anion is observed in the analogous $(Me_4NSeCN)(p\text{-}C_6F_4I_2)_2$, compound **1**, and indeed compounds **1** and **4** pack in different space groups (Table 1). Compound **1** crystallizes in the monoclinic system with the $P2_1/n$ space group. The $C_6F_4I_2$ molecules are aligned in columns along the *a* axis and are connected through the *b* axis by halogen bonding interactions. The cations (Me_4N^+) alternate with the $SeCN^-$ anions between the $C_6F_4I_2$ molecules (Figures S4 and S5, see Supporting Information). Out of the four halogen bonds per selenocyanate anion, three are interactions between iodine and selenium (a trifurcated bond), and one is between nitrogen and a single iodine (Figure 1c). Analogously, Cinčić et al. observed trifurcated bonds associated with four-centered interactions at the sulfur atom in metal bonded thiocyanate ions with I···S−C angles of 90°.[55] Cauliez et al. observed a similar phenomenon with thiocyanate in the compound $(Et_4NSCN)_2(p\text{-}C_6F_4I_2)_5$, where the nitrogen interacts with two iodines, while the sulfur interacts with three iodines.[22] One may anticipate that selenocyanate may bind in a similar fashion to thiocyanate, since they are analogues. Again, compound **1** demonstrates strong halogen bonding type interactions, as characterized by short $d_{I\cdots Se}$ (3.393, 3.421, 3.405 Å) and $d_{I\cdots N}$ (3.034 Å) interatomic distances and typical halogen bonding angles involving selenium ($\theta_{I\cdots Se-C}$: 117.7°, 83.9°, 87.0°). Conversely, nitrogen behaves in a somewhat unexpected manner, where the I···N≡C angle observed (125.8°) deviates from what would be expected for a halogen bond with the SCN^- anion. Bock and Holl[23] and Cauliez et al.[22] have observed I···N≡C angles ranging between 145° and 170° and approximately 90° I···S−C angles.

Finally, compound **2** is formed between Me_4NSeCN and *o*-$C_6F_4I_2$, resulting in $(Me_4NSeCN)(o\text{-}C_6F_4I_2)_2$. It crystallizes in a triclinic system with the $P\bar{1}$ space group. The selenium atom interacts with three iodines, forming a trifurcated bond, and nitrogen interacts with a single iodine, similar to what was observed for compound **1** (Figure 1d). The *o*-$C_6F_4I_2$ moieties pack in a staggered column. The Me_4N^+ cation and selenocyanate anion alternate between the *o*-$C_6F_4I_2$ moieties along the *c* axis (Figures S6 and S7, see Supporting Information). Again, the selenocyanate anion adopts specific motifs characterized by short 90° I···Se contacts and I···Se−C angles near 90° ($d_{I\cdots Se}$: 3.404, 3.552, 3.401 Å and $\theta_{I\cdots Se-C}$: 80.95°, 89.95°, and 94.01°), and a nonlinear I···NC contact ($d_{I\cdots N}$: 3.035 Å, $\theta_{I\cdots N-C}$: 124.13°).

2. Solid-State NMR Spectroscopy. *(i). ^{13}C and ^{15}N Chemical Shifts.* Presented in Figure 2 are the thiocyanate and selenocyanate regions of the ^{15}N CPMAS NMR spectra of compounds **1**−**4** as well as simple KSCN, Me_4NSCN, *n*-Bu_4NSCN, and Me_4NSeCN salts for comparison. The isotropic chemical shifts are presented in Table 3, and range from 212.4 ppm for KSCN to 258.3 ppm for $(Me_4NSeCN)(o\text{-}C_6F_4I_2)_2$. Several important points can be made. First, it is observed that for the thiocyanate anion, the ^{15}N chemical shifts in general are somewhat sensitive to the identity of the counterion and to differences in crystal packing in the various compounds. For example, the chemical shifts for Me_4NSCN and *n*-Bu_4NSCN, which have similar ammonium counterions, are comparable (within 1.6 ppm). Second, it is clear that the selenocyanate nitrogen resonance is consistently shifted to higher frequency relative to thiocyanate nitrogens; this is consistent with previous reports, where Bernard et al.[68] observed an increase in the cyanate ^{15}N chemical shift in Me_4NSeCN compared to NH_4SCN of 44 ppm, and also compared two previous solution ^{15}N NMR studies of selenocyanate[56] and thiocyanate[57] ions and noted analogous increases of 30 ppm. It is also observed that the addition of a halogen bonding interaction to the thiocyanate nitrogen environment results in a small but measurable shift of the cyanate ^{15}N resonance to lower frequency; this shift is 4.5 ppm for the *n*-$Bu_4NSCN/(n\text{-}Bu_4NSCN)(p\text{-}C_6F_4I_2)$ pair and 2.5 ppm for the $Me_4NSCN/(Me_4NSCN)(p\text{-}C_6F_4I_2)_2$ pair. Conversely, for

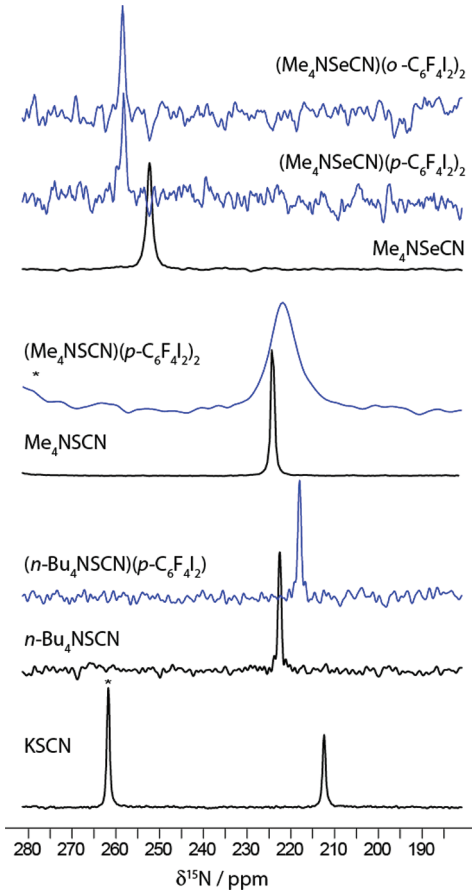

Figure 2. Experimental ^{15}N CPMAS SSNMR spectra acquired at 9.4 T of all SCN^- and $SeCN^-$ salts (black) studied as well as related halogen-containing complexes (blue). KSCN, Me_4NSCN, and **4** are 98%, ∼50%, and <50% labeled with ^{15}N thiocyanate, respectively. The ^{15}N spectra of the other compounds were acquired with ^{15}N in natural abundance. Spinning sidebands are represented by asterisks.

dx.doi.org/10.1021/cg200889y |*Cryst. Growth Des.* 2011, 11, 4984–4995

Table 3. Experimental ^{13}C and ^{15}N Chemical Shift Parameters for Thiocyanate and Selenocyanate Compounds

compound	δ_{iso} (^{13}C)/ ppm	Ω (^{13}C)/ppm	κ (^{13}C)	δ_{iso} (^{15}N)/ppm	Ω (^{15}N)/ppm	κ (^{15}N)
KSCN[a]	139.2(0.4)	327(1)	0.95(0.4)	212.4(0.1)	410(10)	0.96(0.10)
n-Bu_4NSCN	129.4(0.3)	n/a	n/a	222.4(0.4)	n/a	n/a
(*n*-Bu_4NSCN)(*p*-$C_6F_4I_2$)	129.8(0.6)	n/a	n/a	217.9(0.4)	n/a	n/a
Me_4NSCN[a]	128.5(0.1)	296(5)	1.00(0.10)	224.0(0.2)	420(10)	0.96(0.10)
(Me_4NSCN)(*p*-$C_6F_4I_2$)$_2$[a]	131.5(0.5)	302(4)	0.93(0.02)	221.5(0.5)	488(8)	0.94(0.40)
Me_4NSeCN[b]	118.5(0.1)	285(8)	0.98(0.01)	252.2(0.7)	439(10)	1.00(0.03)
(Me_4NSeCN)(*p*-$C_6F_4I_2$)$_2$	113.4(0.4)	n/a	n/a	258.1(0.5)	n/a	n/a
(Me_4NSeCN)(*o*-$C_6F_4I_2$)$_2$	116.1(0.7)	n/a	n/a	258.3(0.6)	n/a	n/a

[a] The thiocyanate groups in KSCN, Me_4NSCN, and (Me_4NSCN)(*p*-$C_6F_4I_2$)$_2$ were isotopically enriched in ^{13}C or ^{15}N. All data in the table are for the thiocyanate and selenocyanate carbons and nitrogens only. [b] Span and skew values determined by Bernard et al.[68]

the selenocyanates, a small increase in the ^{15}N chemical shift is observed for the compounds exhibiting halogen bonding relative to Me_4NSeCN; the shift is 5.9 ppm for the Me_4NSeCN/(Me_4NSeCN)(*p*-$C_6F_4I_2$)$_2$ pair and 6.1 ppm for the Me_4NSeCN/(Me_4NSeCN)(*o*-$C_6F_4I_2$)$_2$ pair. It is not immediately clear why the shifts are in opposite directions for the thiocyanate pairs compared to the selenocyanate pairs, and it is not possible to unequivocally attribute the shifts solely or directly to the presence of a halogen bonding interaction. Undoubtedly, there is an interplay of competing factors which influence the observed shifts; for example, the direct effects of a halogen bonding interaction may compete with concurrent small structural changes in the ions (bond lengths and angles) and with changes in longer-range interactions (i.e., different space groups and crystal packing effects). The promising conclusion from the ^{15}N NMR spectra, however, is that changes are observed in the spectra of compounds exhibiting halogen bonding to nitrogen relative to reference compounds where such interactions are absent. A final point of interest in these spectra is the much broader resonance (250 Hz line width at half-height) observed for (Me_4NSCN)(*p*-$C_6F_4I_2$)$_2$ relative to the other compounds. This is also observed in the ^{13}C NMR spectrum of the same compound (vide infra) and is consistent with the disorder of the thiocyanate ion noted from the X-ray crystallography studies (vide supra). To aid in confirming that the broadened peaks could be attributed to disorder, calculations (B3LYP/3-21G) were performed on the two closest isolated thiocyanate anions (5.8 Å between the two nitrogen atoms) from adjacent unit cells. Two environments were studied, where one SCN^- was kept in a fixed position and the second SCN^- was flipped in each of the two possible orientations. This rudimentary calculation permitted to see if one could expect a measurable chemical shift difference as a result of disorder. Calculations demonstrated that the magnetic shielding constant, σ_{iso}, varies by 1 ppm for ^{15}N. This is consistent with the breadth of the peak observed experimentally for ^{15}N.

Since the isotropic chemical shift represents an average of the three principal components of the CS tensor ($\delta_{iso} = (1/3)(\delta_{11} + \delta_{22} + \delta_{33})$; see also Supporting Information), we explored the possibility that more substantial changes in the tensor components were occurring in the presence of halogen bonding. The Me_4NSCN/(Me_4NSCN)(*p*-$C_6F_4I_2$)$_2$ pair was prepared with ^{15}N isotopic enrichment (~50%) at the thiocyanate nitrogen, and spinning sideband manifolds were obtained using CPMAS NMR. The spectra and their corresponding simulations are presented in Figure 3. Whereas the ^{15}N CS tensor span (representative

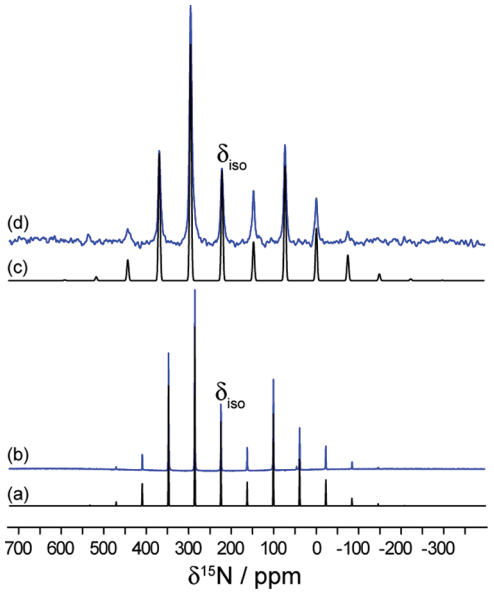

Figure 3. Experimental ^{15}N CPMAS SSNMR spectra acquired at 9.4 T for (b) Me_4NSCN (~50% SCN^- labeled ^{15}N), (d) (Me_4NSCN)-(*p*-$C_6F_4I_2$)$_2$ (<50% SCN^- labeled ^{15}N), and analytical simulations (a) and (c), respectively. Isotropic peaks are indicated (224.0 ppm and 221.5 ppm) with spinning frequencies of 2.5 and 3.0 kHz for (b) and (d), respectively.

of the breadth of the pattern, $\Omega = \delta_{11} - \delta_{33}$) and skew (representative of the asymmetry of the pattern, $\kappa = 3(\delta_{22} - \delta_{iso})/\Omega$) remain constant within experimental error for the simple salts $KSC^{15}N$ (Figure 6b) and $Me_4NSC^{15}N$, a non-negligible increase in the span from 420 to 488 ppm is observed for the Me_4NSCN/(Me_4NSCN)(*p*-$C_6F_4I_2$)$_2$ pair. While this change must be due to the change in environment around the thiocyanate nitrogen, it is difficult to interpret the results further in terms of halogen bonding, given the relatively small changes in each of the principal components of the CS tensor and also given the disorder of the SCN^- ion. Furthermore, it may be seen in Figure 3d that each of the spinning sidebands are broadened (250 Hz at half-height) for (Me_4NSCN)(*p*-$C_6F_4I_2$)$_2$ relative to those for Me_4NSCN (40 Hz at half-height), which may decrease the precision of the reported numbers for the former compound. The observed broadening, however, is again consistent with disorder of the SCN^- ions in (Me_4NSCN)(*p*-$C_6F_4I_2$)$_2$.

The thiocyanate and selenocyanate carbon region of the ^{13}C CPMAS NMR spectra of compounds **1**−**4** as well as KSCN,

Me_4NSCN, *n*-Bu_4NSCN, and Me_4NSeCN are shown in Figure 4. As for ^{15}N, changes in chemical shifts are small but measurable when comparing a simple salt to the analogous halogen-bonded compound. In direct opposition to the ^{15}N chemical shifts, we observe that the

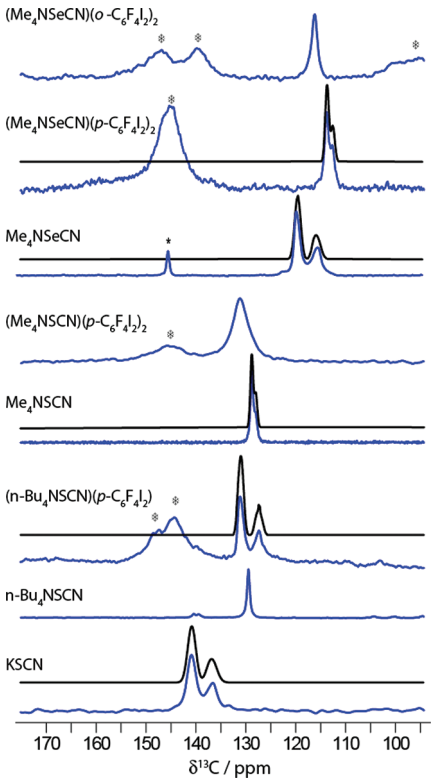

Figure 4. ^{13}C CPMAS SSNMR spectra (blue) of all R_4NSCN, R_4NSeCN, and related halogen-containing complexes. Spinning sidebands are indicated with asterisks and the aromatic carbon resonances are indicated by snowflakes. Spectra were acquired at either 4.7 T (KSCN (99.99% ^{13}C), Me_4NSCN (42% ^{13}C), *n*-Bu_4NSCN, Me_4NSeCN) or 9.4 T (compounds **1, 2, 3,** and **4** (<42% ^{13}C)) using proton decoupling (SPINAL-64). Residual dipolar coupling between ^{14}N ($I = 1$) and ^{13}C ($I = 1/2$) of the SCN^- or $SeCN^-$ anion is observed for certain compounds. The simulations of the isotropic peak are done using WSOLIDS1 under the assumption of an infinite MAS rate (black). The values of $C_Q(^{14}N)$, R_{DD}, and the ^{13}C chemical shifts may be found in Tables 3 and 4.

^{13}C chemical shift for the thiocyanate ion *increases* slightly in the presence of halogen bonding, and the ^{13}C chemical shift for the selenocyanate ion *decreases* slightly in the presence of halogen bonding (Table 3). For example, for the $Me_4NSCN/(Me_4NSCN)(p\text{-}C_6F_4I_2)_2$ pair this shift is 3.0 ppm, and for the $Me_4NSeCN/(Me_4NSeCN)(p\text{-}C_6F_4I_2)_2$ pair it is 5.1 ppm. It is not surprising that the ^{13}C chemical shifts change minimally for a given pair of compounds since the carbon atom is in the center of the thiocyanate and selenocyanate ions, and therefore is not directly interacting with a halogen atom. Interestingly, Kargol et al. have observed with ^{13}C solution NMR a change in chemical shift in analogous coordinated thiocyanate and selenocyanate metal complexes.[58]

(ii). $^{13}C-^{14}N$ Dipolar Coupling and Comments on ^{14}N Solid-State NMR. In 1982, Zumbulyadis and Gysling[59] reported an unusually narrow ^{13}C NMR spectrum for a static powdered sample of KSCN. The lack of a broad well-defined powder pattern was attributed to rapid motion of the thiocyanate ion; however, we suspect their sample was hydrated. We were able to acquire the proper ^{13}C NMR spectrum for powdered $KS^{13}CN$ (Figure 5) and fit it to determine the ^{13}C CS tensor parameters as well as the effective $^{14}N,^{13}C$ dipolar coupling constant and carbon−nitrogen bond length (Table 4). The analogous experiment was performed for isotopically enriched $(Me_4NS^{13}CN)(p\text{-}C_6F_4I_2)_2$, and the $^{14}N-^{13}C$ bond length was determined to be 1.25 Å, in excellent agreement with the X-ray value we measured (1.242 Å). This suggests that the thiocyanate disorder in this compound is static rather than dynamic, as no averaging of the static dipolar coupling tensor is observed. Although ^{13}C isotopic enrichment of all compounds in this paper was beyond the scope of the current study, the good quality of the spectra and the quantitative agreement between NMR and X-ray methods for measuring selected internuclear distances demonstrates the potential of multinuclear solid-state magnetic resonance for further studies of halogen bonding interactions. This may be particularly useful in cases where single crystals or good quality diffraction data are difficult to obtain.

There is a 2:1 doublet-like structure observed in most of the ^{13}C CPMAS NMR spectra (Figure 4). It is well-known that MAS does not entirely average the dipolar coupling between a spin-1/2 nucleus (such as ^{13}C) and a quadrupolar nucleus (such as ^{14}N) to zero.[60,61] For this reason, residual dipolar coupling (RDC) is often observed in the ^{13}C CPMAS NMR spectra of ^{13}C spins which are coupled to ^{14}N; this is the origin of the 2:1 doublets. Simulation of these lineshapes[62] depends on the dipolar coupling

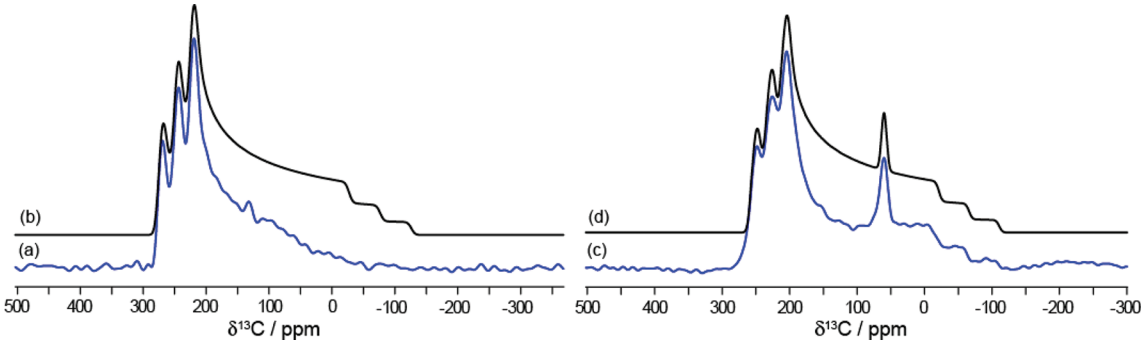

Figure 5. Experimental (a) and simulated ^{13}C SSNMR spectra (b) of KSCN (99.99% ^{13}C) under stationary conditions using a Hahn echo (i.e., $\pi/2\text{-}\tau_1\text{-}\pi\text{-}\tau_2$-acq) pulse sequence. Experimental ^{13}C CP SSNMR spectrum of a stationary sample of <42% ^{13}C-enriched $(Me_4NS^{13}CN)(p\text{-}C_6F_4I_2)_2$ (c) and simulated spectrum (d). The peak at ~60 ppm corresponds to the methyl groups. Both ^{13}C SSNMR spectra were acquired at 4.7 T. Difficulties in observing the three "step" discontinuities experimentally in (a) are attributed to anisotropic spin−lattice relaxation.

Table 4. Experimental Thiocyanate and Selenocyanate ^{14}N,^{13}C Dipolar Couplings and ^{14}N Quadrupolar Coupling Data Obtained from Solid-State NMR Spectroscopy and X-ray Data[a]

		SSNMR		X-ray	
compound	C_Q (^{14}N)/MHz	R_{DD}/Hz	r_{C-N}/Å[e]	R_{DD}/Hz	r_{C-N}/Å
KSCN[b]	−2.43(0.01)	1246(12)	1.206	1458	1.144
n-Bu_4NSCN[d]	n/a	n/a	n/a	1462	1.143
(*n*-Bu_4NSCN)(*p*-$C_6F_4I_2$)[d]	−1.75(0.05)	1514(10)	1.130	1514	1.130
Me_4NSCN[c]	−2.15(0.10)	1254(15)	1.203	1254	1.203
(Me_4NSCN)(*p*-$C_6F_4I_2$)$_2$[b]	unresolved	1125(10)	1.247	1140	1.242
Me_4NSeCN[b]	−2.60(0.20)	1180(30)	1.228	1538	1.113
(Me_4NSeCN)(*p*-$C_6F_4I_2$)$_2$[c]	−2.55(0.20)	1428(7)	1.152	1428	1.152
(Me_4NSeCN)(*o*-$C_6F_4I_2$)$_2$[d]	unresolved	n/a	n/a	1460	1.144

[a] The EFG tensor, **V**, can be diagonalized to provide three principal components defined as $|V_{33}| \geq |V_{22}| \geq |V_{11}|$. Quadrupolar coupling constant: $C_Q = eQV_{33}/h$. Dipolar coupling constant: see eq 2. [b] These compounds have ^{13}C static SSNMR spectra; in these cases the dipolar coupling constant, R_{DD}, is directly extracted from the spectra. [c] ^{13}C SSNMR experiments on static samples were *not* carried out in these cases; therefore, R_{DD} is fixed at the value determined from the crystal structure and the value of C_Q is determined from SSNMR with the angles $\beta = \alpha = 0°$. [d] No residual dipolar coupling is observed for these compounds in their ^{13}C CPMAS NMR spectra. [e] Distances are calculated under the assumption of negligible motional averaging of R_{DD} and also under the assumption of a negligible indirect nuclear spin−spin coupling tensor anisotropy (ΔJ). For these reasons, it is difficult to assign precise error bars to the r_{CN} data.

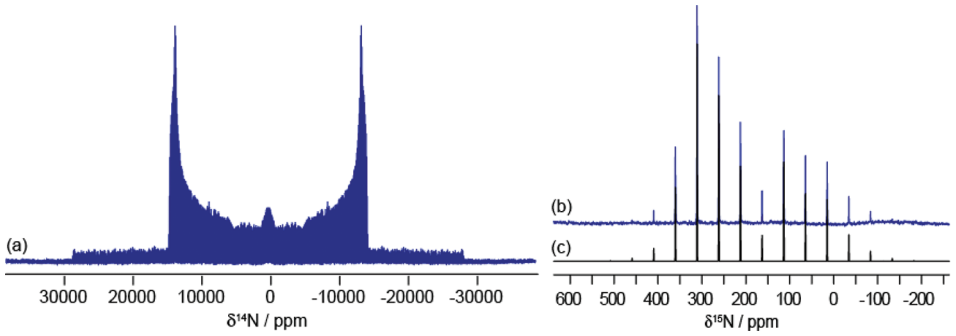

Figure 6. Experimental ^{14}N WURST-QCPMG SSNMR spectrum of KSCN acquired at 21.1 T (a). The ^{14}N spectrum was obtained by acquiring only half of the spectral region and symmetrizing it. This approach is only valid if the chemical shift anisotropy is negligible compared to the breadth of the of the spectrum. Experimental ^{15}N CPMAS SSNMR spectrum of labeled ^{15}N (>98%) KSCN acquired at 9.4 T (b) and simulated spectrum (c).

constant between the two spins, the quadrupolar coupling constant (C_Q) of the ^{14}N, and the orientation of the ^{14}N electric field gradient (EFG) with respect to the $^{14}N-^{13}C$ dipolar tensor. The frequency shift $\nu_I(m_S)$ is expressed in eq 1,

$$\nu_I(m_S) = \frac{3R_{DD}C_Q^S}{20\nu_0^S}\left[\frac{S(S+1)-3m_S^2}{S(2S+1)}\right][3\cos^2\beta_D - 1 + 2\eta_Q^S \sin^2\beta_D \cos^2 2\alpha_D] \quad (1)$$

$$R_{DD} = \frac{\mu_0}{4\pi}\frac{\hbar\gamma_S\gamma_I\langle r^{-3}\rangle}{2\pi} \quad (2)$$

which depends on $C_Q{}^S$ (the quadrupolar coupling constant of the coupled nucleus (S)), S is the spin of the coupled nucleus, $\nu_0{}^S$ is its Larmor frequency, m_S is the spin state of the coupled nucleus, the angles β_D, α_D are those which relate the dipolar principal axis system (PAS) to the EFG PAS, R_{DD} is the dipolar coupling constant (eq 2), which depends on the motionally averaged inverse cube of the internuclear distance between the nuclei, $\hbar$ is the reduced Planck constant, γ are the magnetogyric ratios, and μ_0 is the permeability constant. In the case of SCN^- and $SeCN^-$ ions, it is reasonable to assume that the largest component of the ^{14}N EFG tensor will be coincident with the unique component of the dipolar tensor since the ions maintain local pseudo-C_∞ symmetry in the complexes; hence, the angles α_D and β_D were fixed to zero. Furthermore, in many cases the dipolar coupling constant may be calculated directly from the X-ray coordinates of the two coupled nuclei, that is, independently of the NMR experiment. However, the value $R_{DD}(^{14}N,^{13}C)$ can be extracted from a ^{13}C spectrum of a stationary powdered sample (demonstrated in the Supporting Information), for compound **4** and KSCN. This leaves the ^{14}N quadrupolar coupling constant and asymmetry parameter as the only unknown parameters, and it is clear that the asymmetry parameter must be close to zero for linear ions (and when $\beta_D = 0$, there is no spectral dependence on η_Q). The fits of the 2:1 doublets in the MAS NMR spectra therefore provide some new information on the value of C_Q-(^{14}N). The data are presented in Table 4.

The measurement of a more complete set of $C_Q(^{14}N)$ values was pursued through the direct observation of the ^{14}N SSNMR spectra. We were able to record a spectrum for KSCN and to determine that the value of $C_Q(^{14}N)$ was consistent with that obtained through the analysis of the residual dipolar coupling in the ^{13}C NMR spectrum (Figure 6a). Here, due to the breadth of

dx.doi.org/10.1021/cg200889y |*Cryst. Growth Des.* 2011, 11, 4984–4995

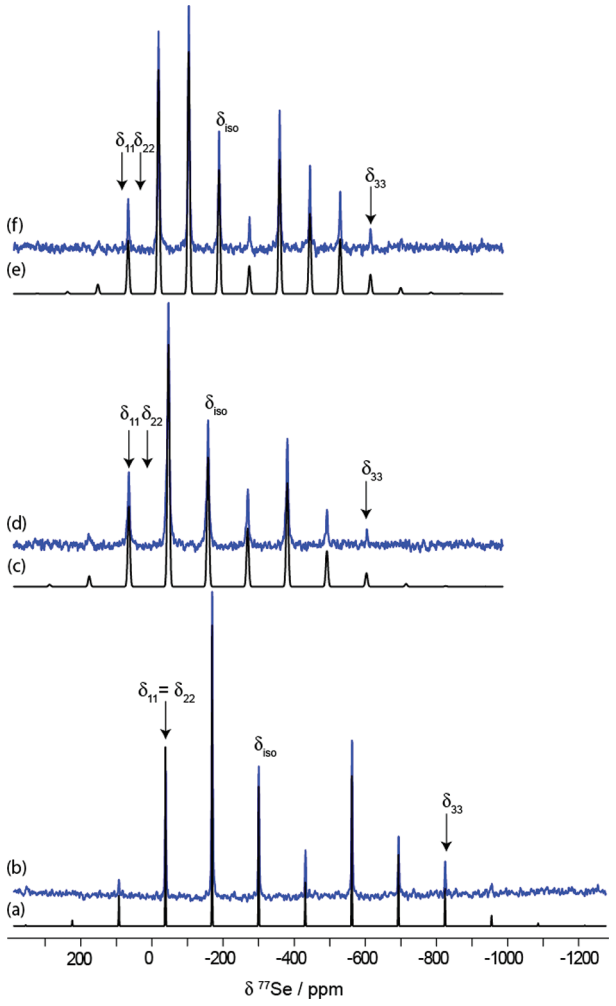

Figure 7. Experimental ^{77}Se CPMAS SSNMR spectra acquired at 9.4 T for (b) Me_4NSeCN (d) $(Me_4NSeCN)(p\text{-}C_6F_4I_2)_2$, (f) $(Me_4NSeCN)(o\text{-}C_6F_4I_2)_2$, and simulated spectra (a), (c), and (e), respectively. Isotropic peaks are indicated (−299.9 ppm, −158.2 ppm, and −189.0 ppm, respectively). Spinning frequencies of 10 kHz, 8.5 kHz, and 6.0 kHz were used for (b), (d), and (f), respectively.

the ^{14}N NMR spectrum, only half of the spectrum was acquired and symmetrization was used to produce the other half. This procedure assumes that the nitrogen chemical shift anisotropy is negligible compared to the breadth of the ^{14}N powder pattern. As shown in the ^{15}N NMR spectrum in Figure 6b, the nitrogen CSA is certainly measurable but very small compared to the breadth of the ^{14}N powder pattern shown in Figure 6a. As a result, this measurement of $C_Q(^{14}N)$ for KSCN is not extremely precise but useful to show consistency with the value inferred from the ^{13}C MAS NMR spectroscopy (vide supra). ^{14}N WURST-QCPMG SSNMR experiments are technically challenging and importantly require a long enough ^{14}N T_2 relaxation time constant. Attempts to record ^{14}N WURST-QCPMG SSNMR spectra of $n\text{-}Bu_4NSCN$ at 21.1 T and a larger series of the compounds in Table 4 at 9.4 and 11.7 T were unsuccessful, and we attribute the lack of signal to a short ^{14}N T_2, likely due to molecular motion and/or due to ^{14}N−^{19}F and ^{14}N−^{127}I dipolar couplings which are absent in the model compound KSCN. Thus, while the ^{14}N quadrupolar coupling constant provides additional information on the nitrogen environment in thiocyanate and selenocyanate compounds, it is currently impractical to acquire these data for most of the compounds in Table 4 through direct wide-line ^{14}N NMR spectroscopy.

(iii). ^{77}Se SSNMR. The ^{77}Se nucleus (n.a. 7.63%) is known for large CSA[37] and long T_1 relaxation times.[63,64] Selenium solid-state NMR[65] provides a particularly sensitive probe of molecular structure as it exhibits a large chemical shift range of over 3000 ppm.[66,67] As discussed above, the X-ray crystal structures obtained for $(Me_4NSeCN)(p\text{-}C_6F_4I_2)_2$ and $(Me_4NSeCN)(o\text{-}C_6F_4I_2)_2$ feature a trifurcated halogen bonding interaction between each Se and three iodines, at distances less than the sum of their van der Waals radii and at angles near 90°. For these reasons, we used ^{77}Se CPMAS NMR experiments to study the selenium environment in the halogen-bonded complexes and compare the results to those for Me_4NSeCN and other benchmark data reported by Bernard et al.[68]

Shown in Figure 7 are the ^{77}Se CPMAS NMR spectra of Me_4NSeCN, $(Me_4NSeCN)(p\text{-}C_6F_4I_2)_2$, and $(Me_4NSeCN)(o\text{-}C_6F_4I_2)_2$. The spectra are of good quality and exhibit spinning sideband manifolds typical of a spin-1/2 nucleus. For Me_4NSeCN, a span of the ^{77}Se CS tensor of 854 ppm is measured; axial symmetry of the tensor is also noted. The axial symmetry is consistent with the near-C_∞ symmetry of the $SeCN^-$ ion in this compound. The value for the span is consistent with the values reported for a series of similar selenocyanates by Bernard et al. Their work also showed that, although there are small variations in the ^{77}Se CS tensor principal components which may be correlated with changes in electronic structure, overall the values of Ω do not vary by more than 70 ppm for a $SeCN^-$ ion in a simple salt.[68]

Most striking therefore is the substantial change in the ^{77}Se NMR spectral parameters in the halogen-bonded complexes compared to the simpler selenocyanate salts (Table 5). As determined through the spectral simulations shown in Figure 7, the span of the CS tensor decreases from 854 ppm in Me_4NSeCN to 642 ppm in $(Me_4NSeCN)(o\text{-}C_6F_4I_2)_2$ and 610 ppm in $(Me_4NSeCN)(p\text{-}C_6F_4I_2)_2$. These changes in span on the order of 25% are substantially more than those observed simply by changing the counterion in simple $SeCN^-$ salts. Inspection of the principal components of the ^{77}Se CS tensors reveals that the component which changes the most is by far the most shielded pseudounique δ_{33} component. The value of δ_{33} changes from −814 ppm in Me_4NSeCN to −611 ppm in $(Me_4NSeCN)(o\text{-}C_6F_4I_2)_2$ and −563 ppm in $(Me_4NSeCN)(p\text{-}C_6F_4I_2)_2$. These changes in the individual principal components explain the marked change in δ_{iso} as well, from −299.4 ppm in Me_4NSeCN to −189.0 ppm in $(Me_4NSeCN)(o\text{-}C_6F_4I_2)_2$ and −158.2 ppm in $(Me_4NSeCN)(p\text{-}C_6F_4I_2)_2$.

Bernard et al.[68] have presented an analysis of selenium CS tensors in the context of Ramsey's theory[69] of magnetic shielding. They showed how the paramagnetic part of the selenium shielding tensor changes in accordance with a small change in the energy gap between the occupied and unoccupied molecular orbitals (MOs) in the $SeCN^-$ ion. For a linear molecule or ion with cylindrical symmetry, that is, C_∞, the shielding tensor will be axially symmetric with the unique component along the symmetry axis. Furthermore, since the contributions to paramagnetic shielding are zero along the symmetry axis, it is generally the case that the unique component is the one which is most shielded, that is, σ_{33}; this corresponds to the smallest component of the chemical shift tensor, that is, δ_{33}. According to Ramsey's theory, it is the mixing of occupied and virtual orbitals in the plane perpendicular to the principal axis

Table 5. Experimental and Calculated[a] ^{77}Se CS Tensors[b] for Selenocyanate Compounds

compound	method	δ_{iso}/ppm	Ω/ppm	κ	δ_{11}/ppm	δ_{22}/ppm	δ_{33}/ppm
Me_4NSeCN[c]	expt	−299.4	854	1	−40	−40	−814
	calc	−551.8	1095	0.99	−179.8	−180.7	−1295
$(Me_4NSeCN)(p\text{-}C_6F_4I_2)_2$	expt	−158.2(0.2)	610(5)	0.98(0.02)	47(5)	41(7)	−563(2)
	calc	−122.5	463	0.82	49	6	−422
$(Me_4NSeCN)(o\text{-}C_6F_4I_2)_2$	expt	−189.0(0.1)	642(8)	0.93(0.01)	31(1)	13(2)	−611(4)
	calc	−180.7	468	0.71	2	−69	−475

[a] B3LYP/6-311++G** (Se, N, C, F), 6-311G**(I) calculation. [b] CS tensors: isotropic chemical shift: $\delta_{iso} = (\delta_{11} + \delta_{22} + \delta_{33})/3$, span: $\Omega \approx \delta_{11} - \delta_{33}$, skew: $\kappa = 3(\delta_{22} - \delta_{iso})/\Omega$, where $\delta_{11} \geq \delta_{22} \geq \delta_{33}$. [c] Values established by Bernard et al. where they estimate errors less than 0.5 ppm for δ_{iso}; those of the individual components are estimated to be on the order of 2−3% of the total span of the tensor. We reproduced these values independently (see Figure 7b).

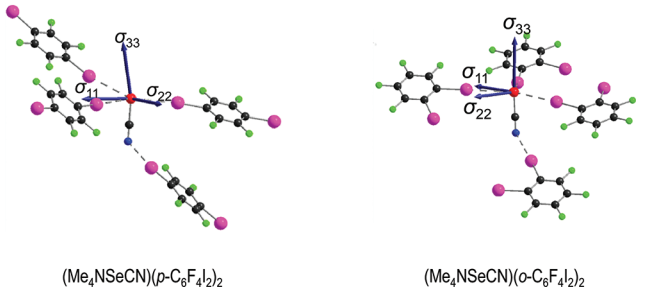

Figure 8. Calculated selenium magnetic shielding tensor orientations for **1** $(Me_4NSeCN)(p\text{-}C_6F_4I_2)_2$ and **2** $(Me_4NSeCN)(o\text{-}C_6F_4I_2)_2$. Selenocyanate being a linear anion results in selenium having C_∞ site symmetry when the ion is isolated. Note that in the limit that $\kappa = +1$, the computed directions of σ_{11} and σ_{22} are not meaningful. For the compounds shown here, C_∞ site symmetry is not strictly maintained, and there are thus small but measurable deviations from axial symmetry in the chemical shift and magnetic shielding tensors.

corresponding to a particular component which affects the value of that component. Presently, we may therefore attribute the marked reduction in the value of δ_{33} in $(Me_4NSeCN)(o\text{-}C_6F_4I_2)_2$ and $(Me_4NSeCN)(p\text{-}C_6F_4I_2)_2$ to the close iodine−selenium contacts in those compounds, specifically in the plane which is approximately perpendicular to the selenocyanate axis. Furthermore we may speculate that the larger negative paramagnetic contribution to σ_{33} in the *para* compound correlates with the shorter average Se−I distance (3.40 Å) compared to the ortho compound (3.45 Å). These halogen bonding interactions are also reflected in the slight decrease in axial symmetry of the ^{77}Se CS tensor, going from a skew of 1.0 in simple selenocyanate salts to 0.93 in $(Me_4NSeCN)(o\text{-}C_6F_4I_2)_2$.

As the ^{77}Se CS tensors are more responsive to structural changes than are ^{13}C or ^{15}N CS tensors in this study, we carried out B3LYP/6-311++G** computations of the ^{77}Se magnetic shielding tensors using models representative of the Se environment in Me_4NSeCN, $(Me_4NSeCN)(o\text{-}C_6F_4I_2)_2$, and $(Me_4NSeCN)(p\text{-}C_6F_4I_2)_2$. It is satisfying to see that the results, presented in Table 5, clearly reproduce the substantial changes in the CS tensors observed experimentally. The trend in the value of the isotropic chemical shift is also reproduced. The changes are overestimated by the calculations, but the important point is that changes on the order of hundreds of ppm are reproduced, and that it is the δ_{33} component which is mainly responsible for the changes. Reasons for the lack of quantitative agreement with experiment include the approximation of using a cluster model for these calculations, the limited availability of a large basis set for iodine, the exclusion of relativistic effects on iodine, and, for the isotropic chemical shift, uncertainties in the ^{77}Se absolute shielding scale. Several theoretical[70] groups have investigated the chemical shift tensors of selenium to establish an absolute shielding scale.[53] This is not an easy task since selenium has a large chemical shift range (3000 ppm) and may itself be subject to relativistic effects.[71]

Examination of the computed ^{77}Se magnetic shielding tensor orientations in $(Me_4NSeCN)(o\text{-}C_6F_4I_2)_2$ and $(Me_4NSeCN)(p\text{-}C_6F_4I_2)_2$ show that the σ_{33} component remains approximately aligned along the local C_∞ axis of the $SeCN^-$ ion (Figure 8). This supports the arguments made above concerning the effect of the iodines on the δ_{33} component of the CS tensor.

CONCLUSIONS

We have reported on the preparation and characterization by X-ray diffraction and multinuclear solid-state magnetic resonance spectroscopy of novel thiocyanate and selenocyanate compounds exhibiting close contacts which fall under the definition of halogen bonding. Selenocyanates $(Me_4NSeCN)(p\text{-}C_6F_4I_2)_2$ and $(Me_4NSeCN)(o\text{-}C_6F_4I_2)_2$ were prepared and their crystal structures revealed similarities and differences in the halogen bonding motifs for $SeCN^-$ versus the analogous SCN^- compounds described by Cauliez et al.[22] In particular, trifurcated I···$SeCN^-$ close contacts are observed with characteristic bonding angles near 90°. X-ray and ^{13}C/^{15}N solid-state NMR evidence indicates that the thiocyanate moieties in $(Me_4NSCN)(p\text{-}C_6F_4I_2)_2$ exhibit disorder. Also, the thiocyanate anion in compound **4** forms halogen bonds with iodine atoms, where both sulfur and nitrogen exhibit close contacts with two iodines. However, a nonlinear angle is observed for the I···NC interaction (125°).

Over a broader range of thiocyanates, ^{13}C chemical shifts were found to increase slightly in complexes exhibiting halogen bonding relative to reference compounds with only simple counterions, while ^{15}N chemical shifts were found to decrease slightly under the same conditions. The opposite trends are observed for the selenocyanates. Much more substantial changes are observed in both the ^{77}Se isotropic chemical shift and in the pseudounique principal component of the ^{77}Se chemical shift tensor when comparing simple selenocyanates with those where the selenium is engaged in halogen bonding interactions with iodine. These results were interpreted in the context of Ramsey's theory of paramagnetic shielding to show that the iodine−selenium interactions are reflected in the ^{77}Se solid-state NMR

parameters, thereby providing an example of the potential of NMR methods for characterizing halogen bonding interactions in the solid state. The arsenal of modern solid-state NMR methods now available offers a wealth of information that may be complementary to X-ray diffraction studies in studying the magnetic and chemical environments of atoms involved in halogen bonding interactions.

■ ASSOCIATED CONTENT

Supporting Information. Experimental details on sample preparation; cif files for **1**, **2**, and **4**; NMR conventions and background; information on dipolar coupling analysis; figures showing details of the crystal structures for **1**, **2**, and **4**; some additional SSNMR spectra recorded at 11.75 T. This material is available free of charge via the Internet at http://pubs.acs.org.

■ AUTHOR INFORMATION

Corresponding Author

*Tel.: +1 613 562 5800 ext. 2018; fax: +1 613 562 5170; e-mail: dbryce@uottawa.ca.

■ ACKNOWLEDGMENT

D.L.B. thanks the Natural Sciences and Engineering Research Council (NSERC) of Canada for funding. Dr. Victor Terskikh and Dr. Glenn Facey are thanked for technical support, and V.T. is thanked for acquiring the ^{14}N NMR spectrum of KSCN. We are grateful to Frédéric Perras for the synthesis of diammonium selenate. Access to the 900 MHz NMR spectrometer was provided by the National Ultrahigh-Field NMR Facility for Solids (Ottawa, Canada), a national research facility funded by the Canada Foundation for Innovation, the Ontario Innovation Trust, Recherche Québec, the National Research Council Canada, and Bruker BioSpin and managed by the University of Ottawa (www.nmr900.ca). NSERC is acknowledged for a Major Resources Support grant.

■ REFERENCES

(1) Benesi, H. A.; Hildebrand, J. H. *J. Am. Chem. Soc.* **1949**, *71*, 2703–2707.
(2) Hassel, O.; Rømming, C. *Q. Rev. Chem. Soc.* **1962**, *16*, 1–18.
(3) Hassel, O. *Science* **1970**, *17*, 497.
(4) Metrangolo, P.; Meyer, F.; Pilati, T.; Resnati, G.; Terraneo, G. *Angew. Chem., Int. Ed.* **2008**, *47*, 6114–6127.
(5) (a) Lommerse, J. P. M.; Stone, A. J.; Taylor, R.; Allen, F. H. *J. Am. Chem. Soc.* **1996**, *118*, 3108–3116. (b) Landrum, G. A.; Goldberg, N.; Hoffmann, R. *J. Chem. Soc., Dalton Trans.* **1997**, 3605–3613.
(6) Metrangolo, P.; Resnati, G. *Halogen Bonding: Fundamentals and Applications*; Springer: Berlin, 2008.
(7) Politzer, P.; Lane, P.; Concha, M. C.; Ma, Y.; Murray, J. S. *J. Mol. Model* **2007**, *13*, 305–311.
(8) Metrangolo, P.; Neukirch, H.; Pilati, T.; Resnati, G. *Acc. Chem. Res.* **2005**, *38*, 386–395.
(9) Legon, A. C. *Phys. Chem. Chem. Phys.* **2010**, *12*, 7736–7747.
(10) Auffinger, P.; Hays, F. A.; Westhof, E.; Ho, P. S. *Proc. Natl. Acad. Sci. U. S. A.* **2004**, *101*, 16789–16794.
(11) Wojtczak, A.; Cody, V.; Luft, J. R.; Pangborn, W. *Acta Crystallogr. D* **2001**, *57*, 1061–1070.
(12) Bayse, C. A.; Rafferty, E. R. *Inorg. Chem.* **2010**, *49*, 5365–5367.
(13) Hardegger, L. A.; Kuhn, B.; Spinnler, B.; Anselm, L.; Ecabert, R.; Stihle, M.; Gsell, B.; Thoma, R.; Diez, J.; Benz, J.; Plancher, J.-M.; Hartmann, G.; Banner, D. W.; Haap, W.; Diederich, F. *Angew. Chem., Int. Ed.* **2011**, *50*, 314–318.
(14) Metrangolo, P.; Carcenac, Y.; Lahtinen, M.; Pilati, T.; Rissanen, K.; Vij, A.; Resnati, G. *Science* **2009**, *323*, 1461–1464.
(15) Lu, Y.; Shi, T.; Wang, Y.; Yang, H.; Yan, X.; Luo, X.; Jiang, H.; Zhu, W. *J. Med. Chem.* **2009**, *52*, 2854–2862.
(16) Bissantz, C.; Kuhn, B.; Stahl, M. *J. Med. Chem.* **2010**, *53*, 5061–5084.
(17) Chudzinski, M. G.; McClary, C. A.; Taylor, M. S. *J. Am. Chem. Soc.* **2011**, *133*, 10559–10567.
(18) Serpell, C. J.; Kilah, N. L.; Costa, P. J.; Félix, V.; Beer, P. D. *Angew. Chem., Int. Ed.* **2010**, *49*, 5322–5326.
(19) Kilah, N. L.; Wise, M. D.; Serpell, C. J.; Thompson, A. L.; White, N. G.; Christensen, K. E.; Beer, P. D. *J. Am. Chem. Soc.* **2010**, *132*, 11893–11895.
(20) Metrangolo, P.; Resnati, G. *Chem. Eur. J.* **2001**, *7*, 2511–2519.
(21) Yamamoto, H. M.; Kosaka, Y.; Maeda, R.; Yamaura, J.; Nakao, A.; Nakamura, T.; Kato, R. *ACS Nano* **2008**, *2*, 143–155.
(22) Cauliez, P.; Polo, V.; Roisnel, T.; Llusar, R.; Fourmigué, M. *CrystEngComm* **2010**, *12*, 558–566.
(23) (a) Bock, H.; Holl, S. *Z. Naturforsch.* **2002**, *57b*, 713–725. (b) Bock, H.; Holl, S. *Z. Naturforsch.* **2002**, *57b*, 835–842. (c) Bock, H.; Holl, S. *Z. Naturforsch.* **2002**, *57b*, 843–858.
(24) Mulliken, R. S.; Person, W. B. *Molecular Complexes*; Wiley-Interscience: New York, NY, 1969.
(25) Bryce, D. L.; Bernard, G. M.; Gee, M.; Lumsden, M. D.; Eichele, K.; Wasylishen, R. E. *Can. J. Anal. Sci. Spectrosc.* **2001**, *46*, 46–82.
(26) Hartmann, S. R.; Hahn, E. L. *Phys. Rev.* **1962**, *128*, 2042–2053.
(27) Widdifield, C. M.; Bryce, D. L. *J. Phys. Chem. A* **2010**, *114*, 10810–10823.
(28) Bryce, D. L.; Widdifield, C. M.; Chapman, R. P.; Attrell, R. J. Chlorine, Bromine, and Iodine Solid-State NMR. In *NMR of Quadrupolar Nuclei in Solid Materials*; Wasylishen, R. E., Ashbrook, S. E., Wimperis, S., Eds.; John Wiley and Sons: Chichester, UK, 2011, in press, DOI: 10.1002/9780470034590.emrstm1214.
(29) Songstad, J.; Stangeland, L. J. *Acta Chem. Scand.* **1970**, *24*, 804–808.
(30) McCrosky, C. R.; Bergstrom, F. W.; Waitkins, G. *J. Am. Chem. Soc.* **1940**, *62*, 2031–2034.
(31) *APEX Software Suite*, v. 2010; Bruker AXS: Madison, WI, 2005.
(32) Blessing, R. H. *Acta Crystallogr.* **1995**, *A51*, 33–38.
(33) Sheldrick, G. M. *Acta Crystallogr.* **2008**, *A64*, 112–122.
(34) Potrzebowski, M. J.; Tekely, P.; Dusausoy, Y. *Solid State Nucl. Magn. Reson.* **1998**, *11*, 253–257.
(35) Fung, B. M.; Khitrin, A. K.; Ermolaev, K. *J. Magn. Reson.* **2000**, *142*, 97–101.
(36) Srinivasan, P. R.; Lichter, R. L. *J. Magn. Reson.* **1977**, *28*, 227–234.
(37) Collins, M. J.; Ratcliffe, C. I.; Ripmeester, J. A. *J. Magn. Reson.* **1986**, *68*, 172–179.
(38) Bloom, A. L.; Shoolery, J. N. *Phys. Rev.* **1955**, *97*, 1261–1265.
(39) Bennett, A. E.; Rienstra, C. M.; Auger, M.; Lakshmi, K. V.; Griffin, R. G. *J. Chem. Phys.* **1995**, *103*, 6951–6958.
(40) Rothwell, W. P.; Waugh, J. S. *J. Chem. Phys.* **1981**, *74*, 2721–2732.
(41) O'Dell, L. A.; Schurko, R. W. *Chem. Phys. Lett.* **2008**, *464*, 97–102.
(42) Bhattacharyya, R.; Frydman, L. *J. Chem. Phys.* **2007**, *127*, 194503.
(43) Kupče, E.; Freeman, R. *J. Magn. Reson. A* **1995**, *115*, 273–276.
(44) Larsen, F. H.; Jakobsen, H. J.; Ellis, P. D.; Nielsen, N. C. *J. Phys. Chem. A* **1997**, *101*, 8597–8606.
(45) Eichele, K.; Wasylishen, R. E. *WSOLIDS NMR Simulation Package*, Version 1.20.15; Dalhousie University: Halifax, 2001.
(46) Alderman, D. W.; Solum, M. S.; Grant, D. M. *J. Chem. Phys.* **1986**, *84*, 3717–3725.
(47) Herzfeld, J.; Berger, A. E. *J. Chem. Phys.* **1980**, *73*, 6021–6030.
(48) Eichele, K.; Wasylishen, R. E. *HBA: Herzfeld-Berger analysis program*, Version 1.6.14; Dalhousie University: Halifax, 2001.
(49) Massiot, D.; Fayon, F.; Capron, M.; King, I.; Le Calvé, S.; Alonso, B.; Durand, J.-O.; Bujoli, B.; Gan, Z.; Hoatson, G. *Magn. Reson. Chem.* **2002**, *40*, 70–76.
(50) Frisch, M. J.; Trucks, G. W.; Schlegel, H. B.; Scuseria, G. E.; Robb, M. A.; Cheeseman, J. R.; Montgomery, Jr., J. A.; Vreven, T.; Kudin, K. N.; Burant, J. C.; Millam, J. M.; Iyengar, S. S.; Tomasi, J.; Barone, V.; Mennucci, B.; Cossi, M.; Scalmani, G.; Rega, N.; Petersson,

G. A.; Nakatsuji, H.; Hada, M.; Ehara, M.; Toyota, K.; Fukuda, R.; Hasegawa, J.;Ishida, M.; Nakajima, T.; Honda, Y.; Kitao, O.; Nakai, H.; Klene, M.; Li, X.; Knox, J. E.; Hratchian, H. P.; Cross, J. B.; Bakken, V.; Adamo, C.; Jaramillo, J.; Gomperts, R.; Stratmann, R. E.; Yazyev, O.; Austin, A. J.; Cammi, R.; Pomelli, C.; Ochterski, J. W.; Ayala, P. Y.; Morokuma, K.; Voth, G. A.; Salvador, P.; Dannenberg, J. J.; Zakrzewski, V. G.; Dapprich, S.; Daniels, A. D.; Strain, M. C.; Farkas, O.; Malick, D. K.; Rabuck, A. D.; Raghavachari, K.; Foresman, J. B.; Ortiz, J. V.; Cui, Q.; Baboul, A. G.; Clifford, S.; Cioslowski, J.; Stefanov, B. B.; Liu, G.; Liashenko, A.; Piskorz, P.; Komaromi, I.; Martin, R. L.; Fox, D. J.; Keith, T.; Al-Laham, M. A.; Peng, C. Y.; Nanayakkara, A.; Challacombe, M.; Gill, P. M. W.; Johnson, B.; Chen, W.; Wong, M. W.; Gonzalez, C.; Pople, J. A. Gaussian 03, rev. B.03 and C.02; Gaussian, Inc.: Wallingford, CT, 2004.

(51) Becke, A. D. *J. Chem. Phys.* **1993**, *98*, 5648–5652.

(52) Adiga, S.; Aebi, D.; Bryce, D. L. *Can. J. Chem.* **2007**, *85*, 496–505.

(53) Jameson, C. J.; Jameson, A. K. *Chem. Phys. Lett.* **1987**, *135*, 254–259.

(54) Nyburg, S. C.; Faerman, C. H. *Acta Crystallogr., Sect. B* **1985**, *41*, 274–279.

(55) Cinčić, D.; Friščić, T.; Jones, W. *CrystEngComm* **2011**, *13*, 3224–3231.

(56) Akhtar, M. N.; Isab, A. A.; Al-Arfaj, A. R. *J. Inorg. Biochem.* **1997**, *66*, 197–205.

(57) Witanowski, M.; Stefaniak, L.; Szymański, S.; Januszewski, H. *J. Magn. Reson.* **1977**, *28*, 217–226.

(58) Kargol, J. A.; Crecely, R. W.; Burmeister, J. L. *Inorg. Chem.* **1979**, *18*, 2532–2535.

(59) Zumbulyadis, N.; Gysling, H. J. *J. Am. Chem. Soc.* **1982**, *104*, 3246–3247.

(60) Andrew, E. R. *Int. Rev. Phys. Chem.* **1981**, *1*, 195–224.

(61) Eichele, K.; Wasylishen, R. E. *Solid State Nucl. Magn. Reson.* **1992**, *1*, 159–163.

(62) Olivieri, A. C. *J. Magn. Reson.* **1989**, *81*, 201–205.

(63) Dawson, W. H.; Odom, J. D. *J. Am. Chem. Soc.* **1977**, *99*, 8352–8354.

(64) Odom, J. D.; Dawson, W. H.; Ellis, P. D. *J. Am. Chem. Soc.* **1979**, *101*, 5815–5822.

(65) Demko, B. A.; Wasylishen, R. E. *Prog. Nucl. Magn. Reson. Spectrosc.* **2009**, *54*, 208–238.

(66) Duddeck, H. *Prog. Nucl. Magn. Reson. Spectrosc.* **1995**, *27*, 1–323.

(67) Duddeck, H. *Annu. Rep. NMR Spectrosc.* **2004**, *52*, 105–166.

(68) Bernard, G. M.; Eichele, K.; Wu, G.; Kirby, C. W.; Wasylishen, R. E. *Can. J. Chem.* **2000**, *78*, 614–625.

(69) Ramsey, N. F. *Phys. Rev.* **1950**, *78*, 699–703.

(70) (a) Jokisaari, J.; Lazzeretti, P.; Pyykkö, P. *Chem. Phys.* **1988**, *123*, 339–350. (b) Buhl, M.; Thiel, W.; Fleischer, U.; Kutzelnigg, W. *J. Phys. Chem.* **1995**, *99*, 4000–4007. (c) Bühl, M.; Gauss, J.; Stanton, J. F. *Chem. Phys. Lett.* **1995**, *241*, 248–252. (d) Schreckenbach, G.; Ruiz-Morales, Y.; Ziegler, T. *J. Chem. Phys.* **1996**, *104*, 8605–8612.

(71) Nakanishi, W.; Hayashi, S.; Katsura, Y.; Hada, M. *J. Phys. Chem. A* **2011**, *115*, 8721–8730.